Measurement of the B_s mass in $B_s \to J/\psi\phi \to \mu^+\mu^- K^+K^-$, and physics validation with J/ψ events in ATLAS

Maren Ugland

Department of Physics and Technology
University of Bergen

September 23, 2008

Outline

The Standard Model

The Standard Model

The Standard Model is today's basic theory of fundamental matter particles and their interactions.

The Standard Model

The Standard Model is today's basic theory of fundamental matter particles and their interactions.

It attempts to explain all the aspects of particle physics in terms of the properties and interactions of three types of particles:

The Standard Model

The Standard Model is today's basic theory of fundamental matter particles and their interactions.

It attempts to explain all the aspects of particle physics in terms of the properties and interactions of three types of particles:

- Leptons
- Quarks

Matter particles of spin-$\frac{1}{2}$

The Standard Model

The Standard Model is today's basic theory of fundamental matter particles and their interactions.

It attempts to explain all the aspects of particle physics in terms of the properties and interactions of three types of particles:

- Leptons
- Quarks

Matter particles of spin-$\frac{1}{2}$

- Gauge bosons

Force carriers of spin-1

The Standard Model

The Standard Model is today's basic theory of fundamental matter particles and their interactions.

It attempts to explain all the aspects of particle physics in terms of the properties and interactions of three types of particles:

- Leptons
- Quarks

  Matter particles of spin-$\frac{1}{2}$
- Gauge bosons

  Force carriers of spin-1

In the Standard Model all these particles are thought to be elementary.

The Standard Model Matter Particles

- There are 3 generations of matter particles.

The Standard Model Matter Particles

- There are 3 generations of matter particles.

Generation	Leptons	Quarks
I	e, ν_e	u, d
II	μ, ν_μ	c, s
III	τ, ν_τ	t, b

The Standard Model Matter Particles

- There are 3 generations of matter particles.

Generation	Leptons	Quarks
I	e, ν_e	u, d
II	μ, ν_μ	c, s
III	τ, ν_τ	t, b

- The particle masses increase with increasing generation number.

The Standard Model Matter Particles

- There are 3 generations of matter particles.

Generation	Leptons	Quarks
I	e, ν_e	u, d
II	μ, ν_μ	c, s
III	τ, ν_τ	t, b

- The particle masses increase with increasing generation number.
- Only the first generation of particles are stable.

The Standard Model Matter Particles

- Quarks carry colour charge (r, g, b).

The Standard Model Matter Particles

- Quarks carry colour charge (r, g, b).
- The theory states that only colour neutral objects can exist freely.

The Standard Model Matter Particles

- Quarks carry colour charge (r, g, b).
- The theory states that only colour neutral objects can exist freely.
- The quarks are therefore only seen in bound colour neutral states, called *hadrons*.

The Standard Model Matter Particles

- Quarks carry colour charge (r, g, b).
- The theory states that only colour neutral objects can exist freely.
- The quarks are therefore only seen in bound colour neutral states, called *hadrons*.
- Two possible colour neutral combinations of quarks exist:

The Standard Model Matter Particles

- Quarks carry colour charge (r, g, b).
- The theory states that only colour neutral objects can exist freely.
- The quarks are therefore only seen in bound colour neutral states, called *hadrons*.
- Two possible colour neutral combinations of quarks exist:
  - *Mesons* consist of a $q\bar{q}$ pair.

The Standard Model Matter Particles

- Quarks carry colour charge (r, g, b).
- The theory states that only colour neutral objects can exist freely.
- The quarks are therefore only seen in bound colour neutral states, called *hadrons*.
- Two possible colour neutral combinations of quarks exist:
  - *Mesons* consist of a $q\bar{q}$ pair.
  - *Baryons* consist of three quarks of different colour.

The Standard Model Force Carriers

- In the Standard Model there are 3 types of forces:
  - The electromagnetic force
  - The weak force
  - The strong force

The Standard Model Force Carriers

- In the Standard Model there are 3 types of forces:
  - The electromagnetic force
  - The weak force
  - The strong force
- The electromagnetic force is mediated by photons, γ.
  The weak force is mediated by the $W^{\pm}$ and Z^0 bosons.
  The strong force is mediated by gluons, g.

The Standard Model Force Carriers

- In the Standard Model there are 3 types of forces:
  - The electromagnetic force
  - The weak force
  - The strong force
- The electromagnetic force is mediated by photons, γ.
  The weak force is mediated by the $W^{\pm}$ and Z^0 bosons.
  The strong force is mediated by gluons, g.
- The range of each force depends on the mass of the force carrier.

The Standard Model Force Carriers

- In the Standard Model there are 3 types of forces:
  - The electromagnetic force
  - The weak force
  - The strong force
- The electromagnetic force is mediated by photons, γ.
  The weak force is mediated by the $W^{\pm}$ and Z^0 bosons.
  The strong force is mediated by gluons, g.
- The range of each force depends on the mass of the force carrier.
  $m_\gamma = 0 \qquad \Rightarrow$ infinite range

The Standard Model Force Carriers

- In the Standard Model there are 3 types of forces:
  - The electromagnetic force
  - The weak force
  - The strong force
- The electromagnetic force is mediated by photons, γ.
  The weak force is mediated by the $W^{\pm}$ and Z^0 bosons.
  The strong force is mediated by gluons, g.
- The range of each force depends on the mass of the force carrier.

  $m_\gamma = 0$ $\Rightarrow$ infinite range

  $m_{W^\pm} \approx 80.4$ GeV
  $m_{Z^0} \approx 91.2$ GeV $\Rightarrow$ short range ($\sim 10^{-18}$ m)

The Standard Model Force Carriers

- In the Standard Model there are 3 types of forces:
  - The electromagnetic force
  - The weak force
  - The strong force
- The electromagnetic force is mediated by photons, γ.
  The weak force is mediated by the $W^{\pm}$ and Z^0 bosons.
  The strong force is mediated by gluons, g.
- The range of each force depends on the mass of the force carrier.

$m_\gamma = 0$ $\Rightarrow$ infinite range

$m_{W^\pm} \approx 80.4$ GeV
$m_{Z^0} \approx 91.2$ GeV $\Rightarrow$ short range ($\sim 10^{-18}$ m)

$m_g = 0$ $\Rightarrow$ short range ($\sim 10^{-15}$ m)

The Standard Model Force Carriers

- In the Standard Model there are 3 types of forces:
  - The electromagnetic force
  - The weak force
  - The strong force
- The electromagnetic force is mediated by photons, γ.
  The weak force is mediated by the $W^{\pm}$ and Z^0 bosons.
  The strong force is mediated by gluons, g.
- The range of each force depends on the mass of the force carrier.

  $m_\gamma = 0$ $\Rightarrow$ infinite range

  $m_{W^\pm} \approx 80.4$ GeV
  $m_{Z^0} \approx 91.2$ GeV $\Rightarrow$ short range ($\sim 10^{-18}$ m)

  $m_g = 0$ $\Rightarrow$ short range ($\sim 10^{-15}$ m)

  Gluons carry colour charge, and are self-interacting.

The ATLAS Experiment

The LHC

- The Large Hadron Collider (LHC) is a 27 km long accelerator ring housed in an underground tunnel near Geneva.

The LHC

- The Large Hadron Collider (LHC) is a 27 km long accelerator ring housed in an underground tunnel near Geneva.
- It will accelerate protons and provide collisions with center of mass energies of up to 14 TeV.

The LHC

- The Large Hadron Collider (LHC) is a 27 km long accelerator ring housed in an underground tunnel near Geneva.
- It will accelerate protons and provide collisions with center of mass energies of up to 14 TeV.
- The LHC provides collisions for 4 main experiments:

The LHC

- The Large Hadron Collider (LHC) is a 27 km long accelerator ring housed in an underground tunnel near Geneva.
- It will accelerate protons and provide collisions with center of mass energies of up to 14 TeV.
- The LHC provides collisions for 4 main experiments:
  - ALICE
  - LHCb
  - CMS
  - ATLAS

The ATLAS Detector

- The ATLAS detector is a multipurpose detector.

The ATLAS Detector

- The ATLAS detector is a multipurpose detector.
- It has a cylindrical geometry with a diameter of about 22 m and a length of about 44 m.
  The total weight of the detector is about 7000 tonnes.

The ATLAS Detector

- The ATLAS detector is a multipurpose detector.
- It has a cylindrical geometry with a diameter of about 22 m and a length of about 44 m.
  The total weight of the detector is about 7000 tonnes.
- The ATLAS detector consists of four main subsystems:

The ATLAS Detector

- The ATLAS detector is a multipurpose detector.
- It has a cylindrical geometry with a diameter of about 22 m and a length of about 44 m.
  The total weight of the detector is about 7000 tonnes.
- The ATLAS detector consists of four main subsystems:
  - The inner detector
  - The calorimeters
  - The muon spectrometers
  - The magnet systems

The ATLAS Detector Subsystems

The Inner Detector

The inner detector is located closest to the interaction point and provides the highest granularity measurements. It provides high resolution momentum measurements, and is also responsible for the reconstruction of secondary vertices.

The ATLAS Detector Subsystems

The Inner Detector

The inner detector is located closest to the interaction point and provides the highest granularity measurements. It provides high resolution momentum measurements, and is also responsible for the reconstruction of secondary vertices.

The Calorimeters

The calorimeters provide high accuracy energy measurements and distinguishes the hadrons from the electrons and photons in the detector.

The ATLAS Detector Subsystems

The Inner Detector

The inner detector is located closest to the interaction point and provides the highest granularity measurements. It provides high resolution momentum measurements, and is also responsible for the reconstruction of secondary vertices.

The Calorimeters

The calorimeters provide high accuracy energy measurements and distinguishes the hadrons from the electrons and photons in the detector.

The Muon Spectrometers

The muon spectrometer makes up the outermost parts of the detector. Its main task is to identify the muons in the detector, and to measure the muon momenta.

The ATLAS Detector

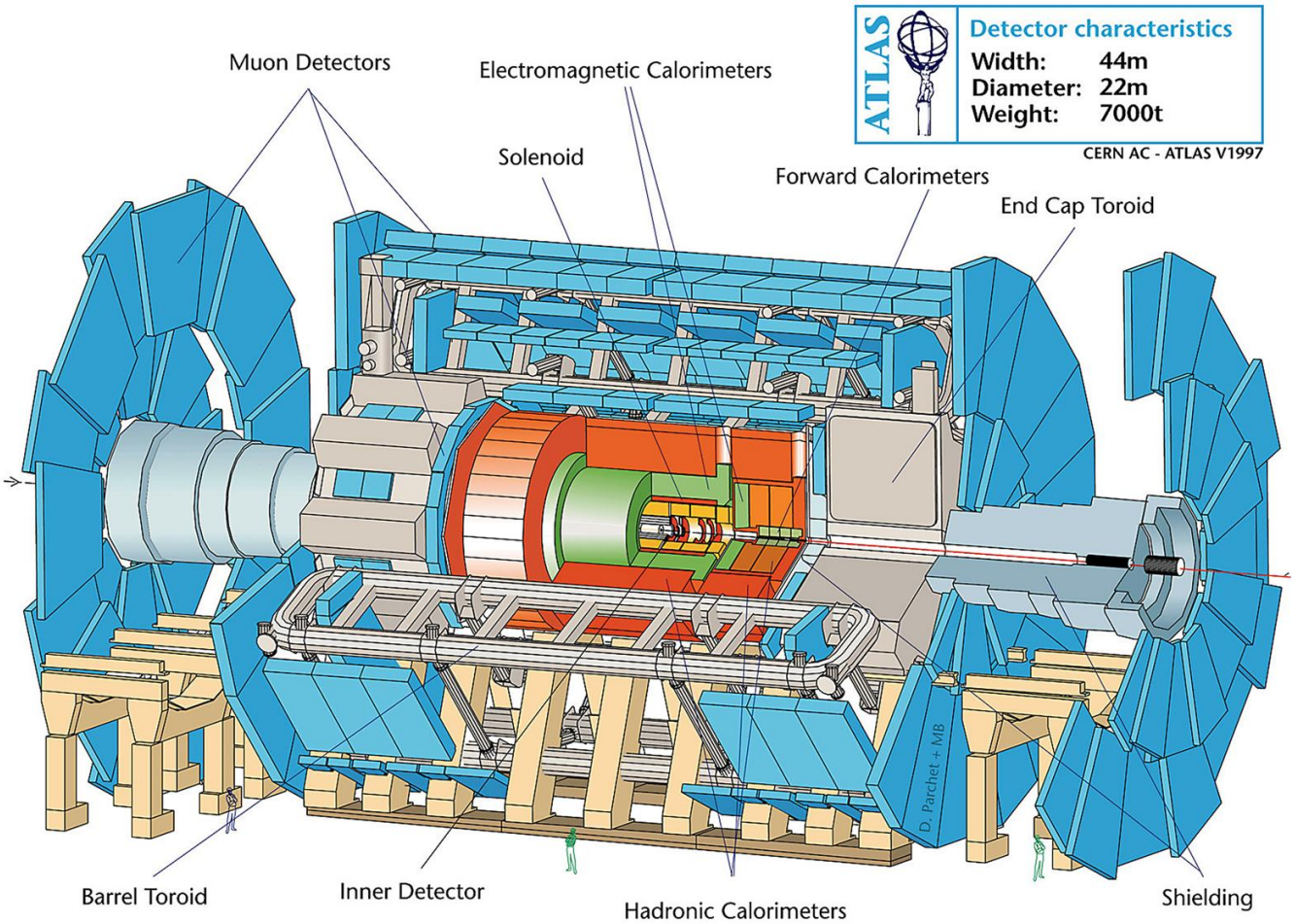

Figure: Overall layout of the ATLAS detector.

Detector Geometry

In order to describe what we see in the ATLAS detector, we define a common (right-handed) coordinate system.

Detector Geometry

In order to describe what we see in the ATLAS detector, we define a common (right-handed) coordinate system.

- The z-axis is given by the beam direction.

Detector Geometry

In order to describe what we see in the ATLAS detector, we define a common (right-handed) coordinate system.

- The z-axis is given by the beam direction.
  The positive x-axis points from the interaction point (IP) towards the center of the LHC ring.

Detector Geometry

In order to describe what we see in the ATLAS detector, we define a common (right-handed) coordinate system.

- The z-axis is given by the beam direction.
  The positive x-axis points from the interaction point (IP) towards the center of the LHC ring.
  The positive y-axis points upwards.

Detector Geometry

In order to describe what we see in the ATLAS detector, we define a common (right-handed) coordinate system.

- The z-axis is given by the beam direction.
  The positive x-axis points from the interaction point (IP) towards the center of the LHC ring.
  The positive y-axis points upwards.
- The azimuthal angle $\phi = \tan^{-1}\left(\frac{p_y}{p_x}\right)$.

Detector Geometry

In order to describe what we see in the ATLAS detector, we define a common (right-handed) coordinate system.

- The z-axis is given by the beam direction.
  The positive x-axis points from the interaction point (IP) towards the center of the LHC ring.
  The positive y-axis points upwards.
- The azimuthal angle $\phi = \tan^{-1}\left(\frac{p_y}{p_x}\right)$.
- The pseudorapidity $\eta = -\ln\left(\tan\left(\frac{\theta}{2}\right)\right)$.

Physics Validation with J/ψ Events in ATLAS

Physics Validation

- Physics validation is an important tool both for simulated and real data. By studying well known structures we acquire valuable insight into the detector performance.

Physics Validation

- Physics validation is an important tool both for simulated and real data. By studying well known structures we acquire valuable insight into the detector performance.
- Simulation studies tell us how well the detector's reconstruction algorithms perform.

Physics Validation

- Physics validation is an important tool both for simulated and real data. By studying well known structures we acquire valuable insight into the detector performance.
- Simulation studies tell us how well the detector's reconstruction algorithms perform.
- The output from real data can be compared to the output from simulated data to make us aware of additional detector effects.

Variations in the J/ψ Mass

- Using 89,000 simulated $J/\psi \rightarrow \mu^+\mu^-$ events, we investigate variations in the J/ψ mass in different detector regions.

Variations in the J/ψ Mass

- Using 89,000 simulated $J/\psi \to \mu^+\mu^-$ events, we investigate variations in the J/ψ mass in different detector regions.
- Since this is a simulation study, we start by examining the reconstruction efficiency:

$$\epsilon = \frac{\#\text{ reconstructed muons}}{\#\text{ generated muons}}$$

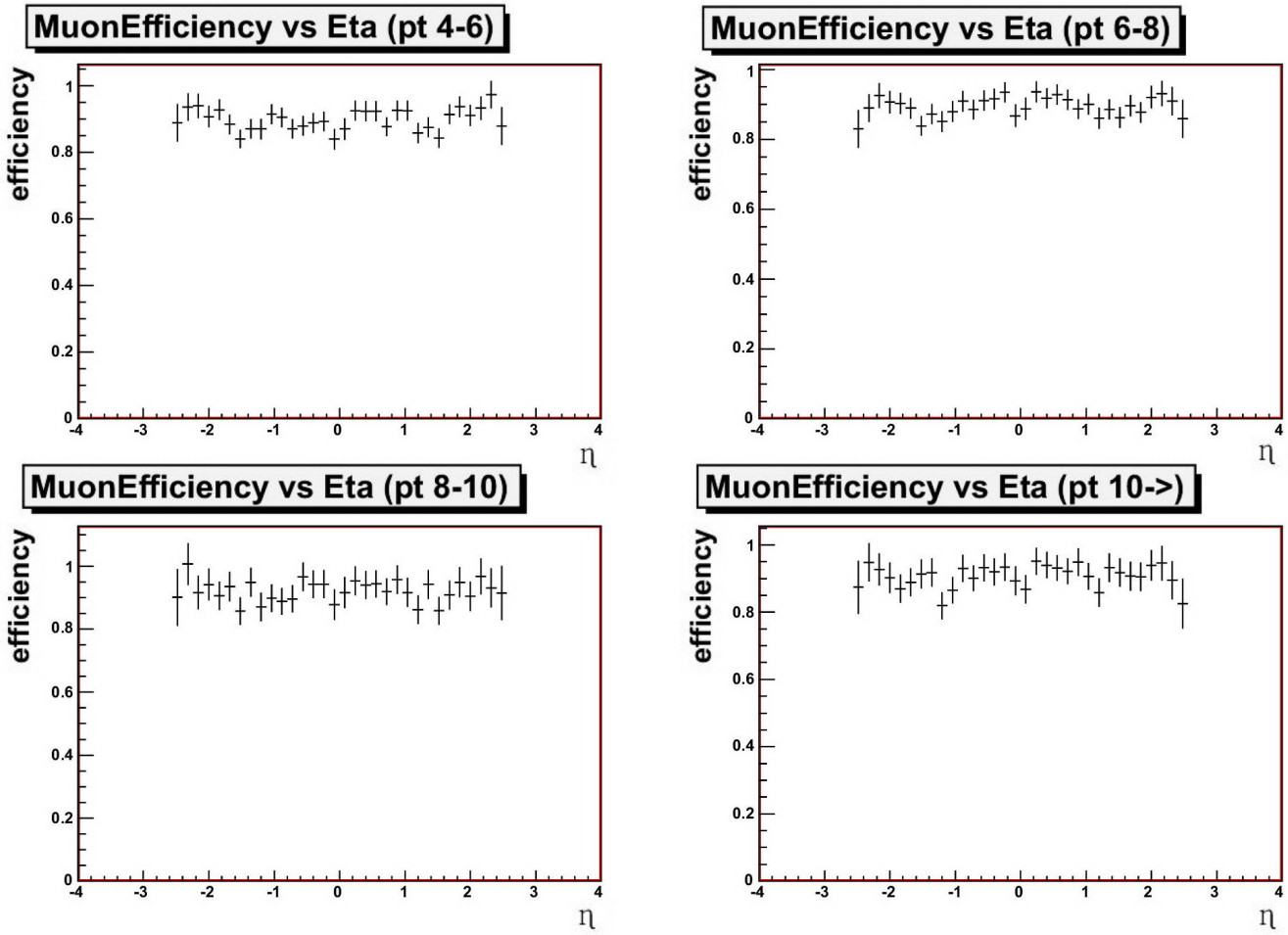

Figure: Muon reconstruction efficiency for different p_T-regions as a function of pseudorapidity

Interpretation of the Efficiency Figures

- The dips around $|\eta| = 0$ and 1.4 correspond to transition regions in the detector.

Interpretation of the Efficiency Figures

- The dips around $|\eta| = 0$ and 1.4 correspond to transition regions in the detector.
  - At zero, the inefficiency is caused by the feet of the detector and by services, like cables and cryogenic lines, to the inner detector.

Interpretation of the Efficiency Figures

- The dips around $|\eta| = 0$ and 1.4 correspond to transition regions in the detector.
  - At zero, the inefficiency is caused by the feet of the detector and by services, like cables and cryogenic lines, to the inner detector.
  - At $|\eta| = 1.4$, it is caused by the extra material introduced at the transition region between the barrel and end-cap components of the calorimeters.

Interpretation of the Efficiency Figures

- The dips around $|\eta| = 0$ and 1.4 correspond to transition regions in the detector.
  - At zero, the inefficiency is caused by the feet of the detector and by services, like cables and cryogenic lines, to the inner detector.
  - At $|\eta| = 1.4$, it is caused by the extra material introduced at the transition region between the barrel and end-cap components of the calorimeters.
- The final dips (at $|\eta| \approx 2.5$) are due to detector limitations in the area close to the beam pipe.

Variations in the J/ψ Mass

- Based on the dips and rises in the efficiency plots, the detector is divided into five positive and five negative η-regions:

Variations in the J/ψ Mass

- Based on the dips and rises in the efficiency plots, the detector is divided into five positive and five negative η-regions:

$$|\eta| \in [0, 0.2), [0.2, 1.3), [1.3, 1.5), [1.5, 2.0), \text{ and } [2.0, \rightarrow)$$

Variations in the J/ψ Mass

- Based on the dips and rises in the efficiency plots, the detector is divided into five positive and five negative η-regions:

$$|\eta| \in [0, 0.2), [0.2, 1.3), [1.3, 1.5), [1.5, 2.0), \text{ and } [2.0, \rightarrow)$$

- In addition, we separate between four different p_T-regions:

Variations in the J/ψ Mass

- Based on the dips and rises in the efficiency plots, the detector is divided into five positive and five negative η-regions:

$$|\eta| \in [0, 0.2), [0.2, 1.3), [1.3, 1.5), [1.5, 2.0), \text{ and } [2.0, \rightarrow)$$

- In addition, we separate between four different p_T-regions:

$$p_T \in [4, 6), [6, 8), [8, 10), \text{ and } [10, \rightarrow)$$

Variations in the J/ψ Mass

- Based on the dips and rises in the efficiency plots, the detector is divided into five positive and five negative η-regions:

$$|\eta| \in [0, 0.2), [0.2, 1.3), [1.3, 1.5), [1.5, 2.0), \text{ and } [2.0, \to)$$

- In addition, we separate between four different p_T-regions:

$$p_T \in [4, 6), [6, 8), [8, 10), \text{ and } [10, \to)$$

- The J/ψ mass is reconstructed, requiring both muons to be in the same η-region.

Variations in the J/ψ Mass

- Based on the dips and rises in the efficiency plots, the detector is divided into five positive and five negative η-regions:

$$|\eta| \in [0, 0.2), [0.2, 1.3), [1.3, 1.5), [1.5, 2.0), \text{ and } [2.0, \to)$$

- In addition, we separate between four different p_T-regions:

$$p_T \in [4, 6), [6, 8), [8, 10), \text{ and } [10, \to)$$

- The J/ψ mass is reconstructed, requiring both muons to be in the same η-region.
- Because of lacking statistics, only one muon is required to be in the desired p_T-region.

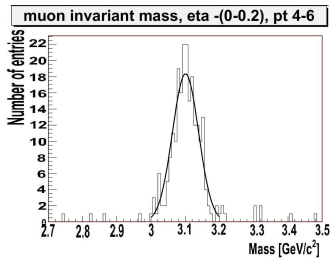
muon invariant mass, eta -(0-0.2), pt 4-6
Number of entries
Mass [GeV/c²]

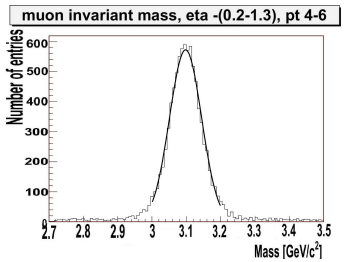
muon invariant mass, eta -(0.2-1.3), pt 4-6
Number of entries
Mass [GeV/c²]

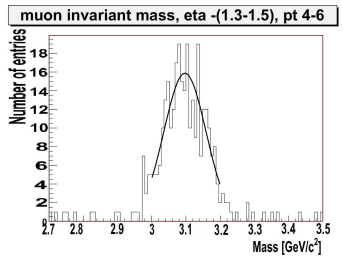
muon invariant mass, eta -(1.3-1.5), pt 4-6
Number of entries
Mass [GeV/c²]

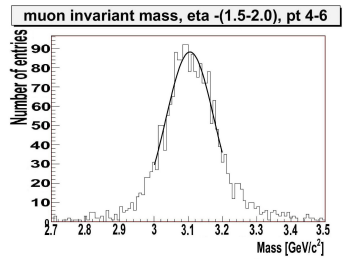
muon invariant mass, eta -(1.5-2.0), pt 4-6
Number of entries
Mass [GeV/c²]

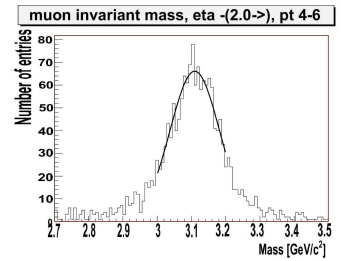
muon invariant mass, eta -(2.0->), pt 4-6
Number of entries
Mass [GeV/c²]

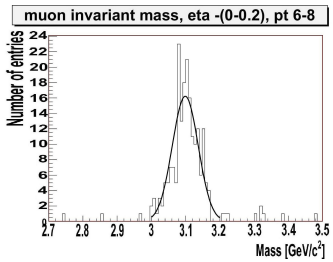
muon invariant mass, eta -(0-0.2), pt 6-8
Number of entries
Mass [GeV/c²]

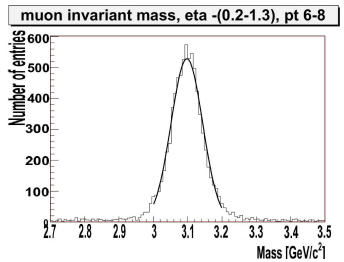
muon invariant mass, eta -(0.2-1.3), pt 6-8
Number of entries
Mass [GeV/c²]

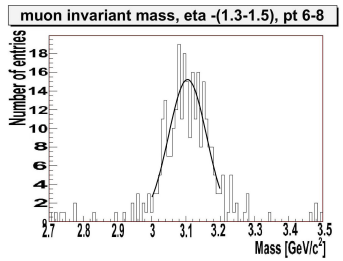
muon invariant mass, eta -(1.3-1.5), pt 6-8
Number of entries
Mass [GeV/c²]

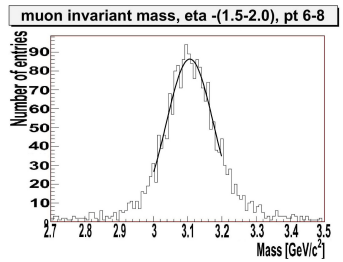
muon invariant mass, eta -(1.5-2.0), pt 6-8
Number of entries
Mass [GeV/c²]

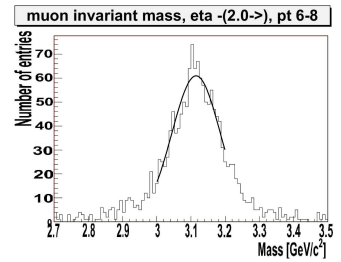
muon invariant mass, eta -(2.0->), pt 6-8
Number of entries
Mass [GeV/c²]

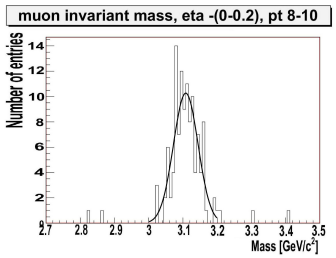
muon invariant mass, eta -(0-0.2), pt 8-10
Number of entries
Mass [GeV/c²]

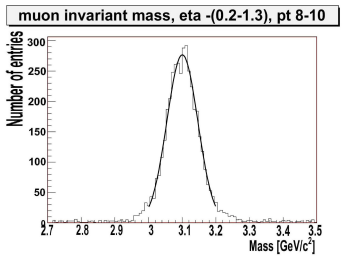
muon invariant mass, eta -(0.2-1.3), pt 8-10
Number of entries
Mass [GeV/c²]

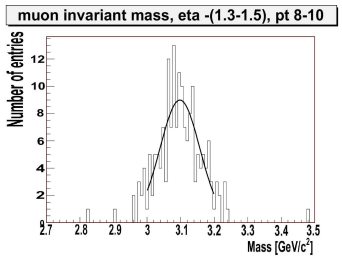
muon invariant mass, eta -(1.3-1.5), pt 8-10
Number of entries
Mass [GeV/c²]

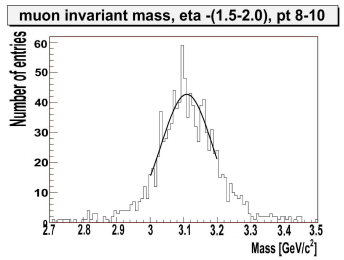
muon invariant mass, eta -(1.5-2.0), pt 8-10
Number of entries
Mass [GeV/c²]

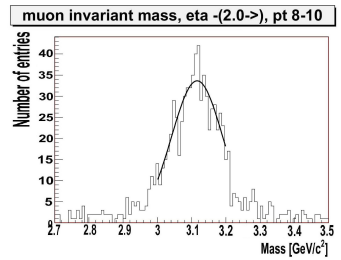
muon invariant mass, eta -(2.0->), pt 8-10
Number of entries
Mass [GeV/c²]

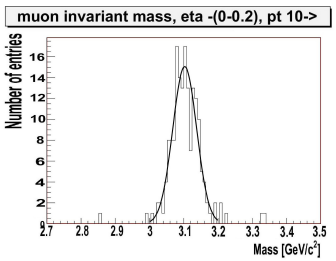
muon invariant mass, eta -(0-0.2), pt 10->
Number of entries
Mass [GeV/c²]

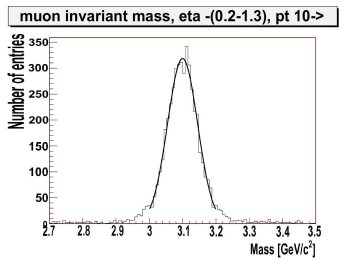
muon invariant mass, eta -(0.2-1.3), pt 10->
Number of entries
Mass [GeV/c²]

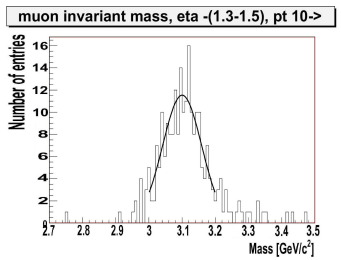
muon invariant mass, eta -(1.3-1.5), pt 10->
Number of entries
Mass [GeV/c²]

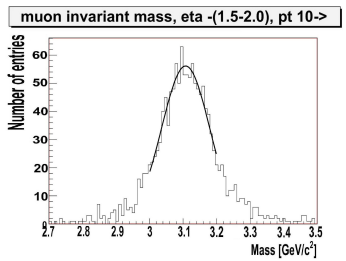
muon invariant mass, eta -(1.5-2.0), pt 10->
Number of entries
Mass [GeV/c²]

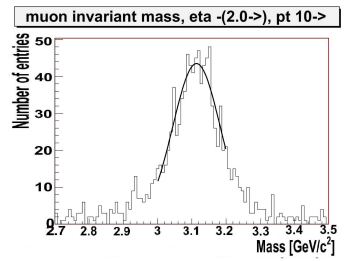
muon invariant mass, eta -(2.0->), pt 10->
Number of entries
Mass [GeV/c²]

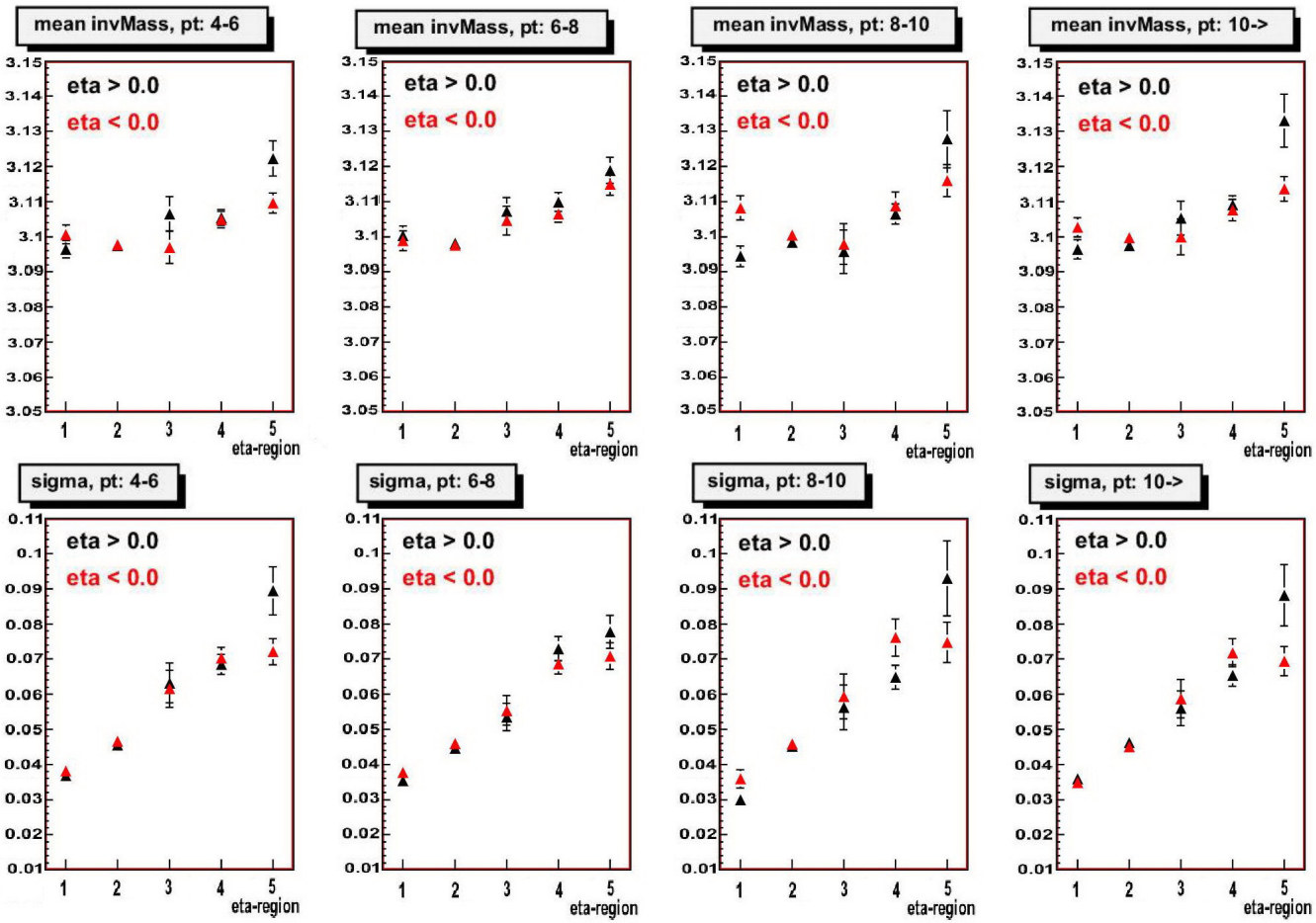

Figure: Summary of the fit results from the previous figure and from a similar collection of plots for regions of positive η, as a function of η-region.

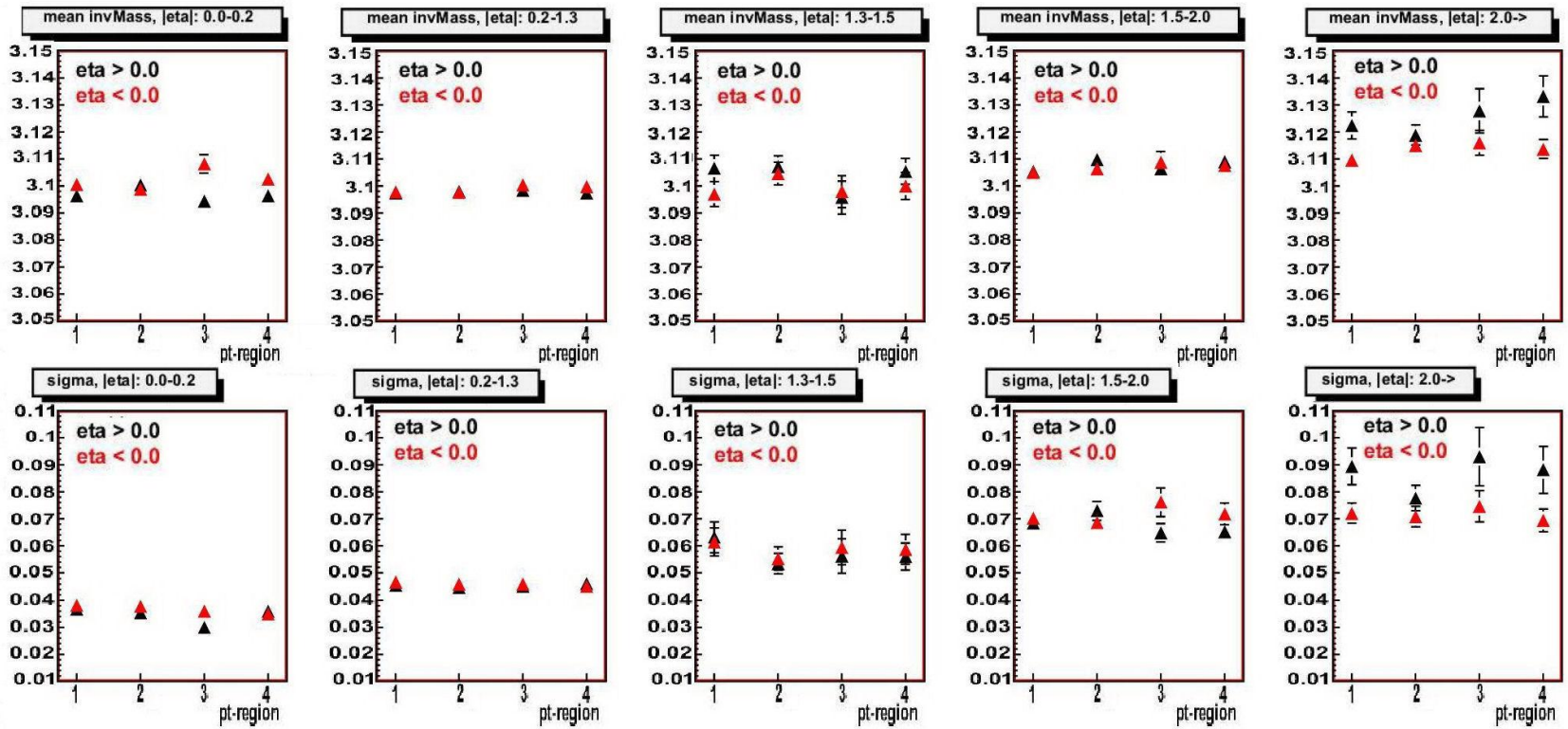

Figure: Summary of the fit results as a function of p_T-region.

Variations in the J/ψ Mass

- The mass and standard deviation becomes larger as $|\eta|$ increases.

Variations in the J/ψ Mass

- The mass and standard deviation becomes larger as $|\eta|$ increases.
- The increasing mass is an effect of an over-correction in the reconstruction algorithms.

Variations in the J/ψ Mass

- The mass and standard deviation becomes larger as $|\eta|$ increases.
- The increasing mass is an effect of an over-correction in the reconstruction algorithms.
- No dependence upon p_T is observed.

Variations in the J/ψ Mass

- The mass and standard deviation becomes larger as $|\eta|$ increases.
- The increasing mass is an effect of an over-correction in the reconstruction algorithms.
- No dependence upon p_T is observed.
- For $|\eta| \in [1.3, 1.5)$ and $[2.0, \rightarrow)$, the reconstructed J/ψ mass seems to be higher in the negative pseudorapidity regions of the detector.

Variations in the J/ψ Mass

- The mass and standard deviation becomes larger as $|\eta|$ increases.
- The increasing mass is an effect of an over-correction in the reconstruction algorithms.
- No dependence upon p_T is observed.
- For $|\eta| \in [1.3, 1.5)$ and $[2.0, \rightarrow)$, the reconstructed J/ψ mass seems to be higher in the negative pseudorapidity regions of the detector.
- This is probably an effect of the low statistics in these regions.

Variations in the J/ψ Mass

- Variations in the J/ψ mass for different regions of $|\phi|$ were also studied.

Variations in the J/ψ Mass

- Variations in the J/ψ mass for different regions of $|\phi|$ were also studied.
- No discrepancy between positive and negative values of ϕ was observed.

Variations in the J/ψ Mass

- Variations in the J/ψ mass for different regions of $|\phi|$ were also studied.
- No discrepancy between positive and negative values of ϕ was observed.
- Only minor fluctuations in the J/ψ mass were seen as a function of $|\phi|$.

Measurement of the B_s Mass in $B_s \to J/\psi\phi \to \mu^+\mu^- K^+K^-$

Reconstructed B_s Mass from the Signal

- The signal sample consists of 14,750 $B_s^0 \rightarrow J/\psi(\mu^+\mu^-)\phi(K^+K^-)$ events.

Reconstructed B_s Mass from the Signal

- The signal sample consists of 14,750 $B_s^0 \rightarrow J/\psi(\mu^+\mu^-)\phi(K^+K^-)$ events.
- Since we are looking at signal only, we first try to reconstruct the B_s mass for "all" combinations of muon and kaon tracks.

Reconstructed B_s Mass from the Signal

- The signal sample consists of 14,750 $B_s^0 \rightarrow J/\psi(\mu^+\mu^-)\phi(K^+K^-)$ events.
- Since we are looking at signal only, we first try to reconstruct the B_s mass for "all" combinations of muon and kaon tracks.

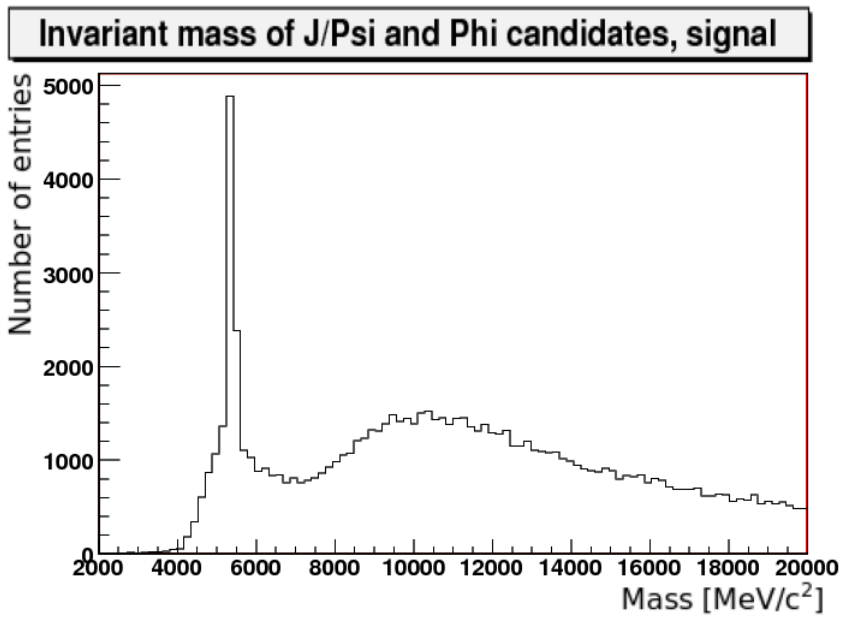

Reconstructed B_s Mass from the Signal

- To clean up the picture, we add some simple requirements:

Reconstructed B_s Mass from the Signal

- To clean up the picture, we add some simple requirements:

Observable	**Criteria**
Muon transverse momentum	$\geq 4 + 6$ GeV
Fit of muon tracks, χ^2/dof	< 4.0
Best vertex quality of B_s, χ^2/dof	—
J/ψ mass	$\mu \pm 3\sigma$ (from fit)
ϕ mass	$\mu \pm 2\sigma$ (from fit)

Reconstructed B_s Mass from the Signal

The J/ψ and ϕ mass were obtained from a Gaussian fit to the invariant $\mu^+\mu^-$ and K^+K^- mass, respectively, after the selection criteria in the table rows above were employed.

Reconstructed B_s Mass from the Signal

The J/ψ and ϕ mass were obtained from a Gaussian fit to the invariant $\mu^+\mu^-$ and K^+K^- mass, respectively, after the selection criteria in the table rows above were employed.

- Obtained: $\mu_{J/\psi} = (3101.7 \pm 0.9)$ MeV ,
  $\sigma_{J/\psi} = (65.34 \pm 0.64)$ MeV.
  PDG value: $m_{J/\psi} = (3096.916 \pm 0.011)$ MeV.

Reconstructed B_s Mass from the Signal

The J/ψ and ϕ mass were obtained from a Gaussian fit to the invariant $\mu^+\mu^-$ and K^+K^- mass, respectively, after the selection criteria in the table rows above were employed.

- Obtained: $\mu_{J/\psi} = (3101.7 \pm 0.9)$ MeV ,
  $\sigma_{J/\psi} = (65.34 \pm 0.64)$ MeV.
  PDG value: $m_{J/\psi} = (3096.916 \pm 0.011)$ MeV.
- Obtained: $\mu_{\phi} = (1019.5 \pm 0.1)$ MeV ,
  $\sigma_{\phi} = (5.104 \pm 0.187)$ MeV.
  PDG value: $m_{\phi} = (1019.455 \pm 0.020)$ MeV.

Reconstructed B_s Mass from the Signal

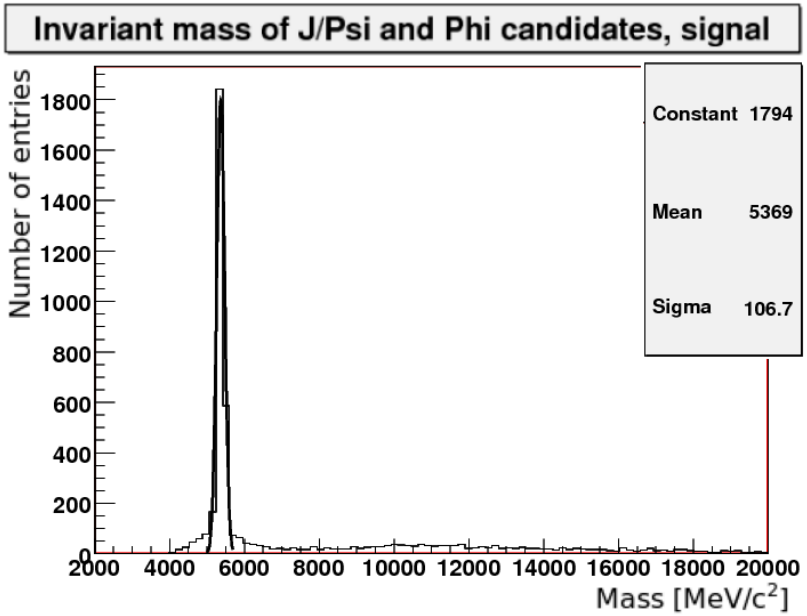

Reconstructed B_s Mass from the Signal

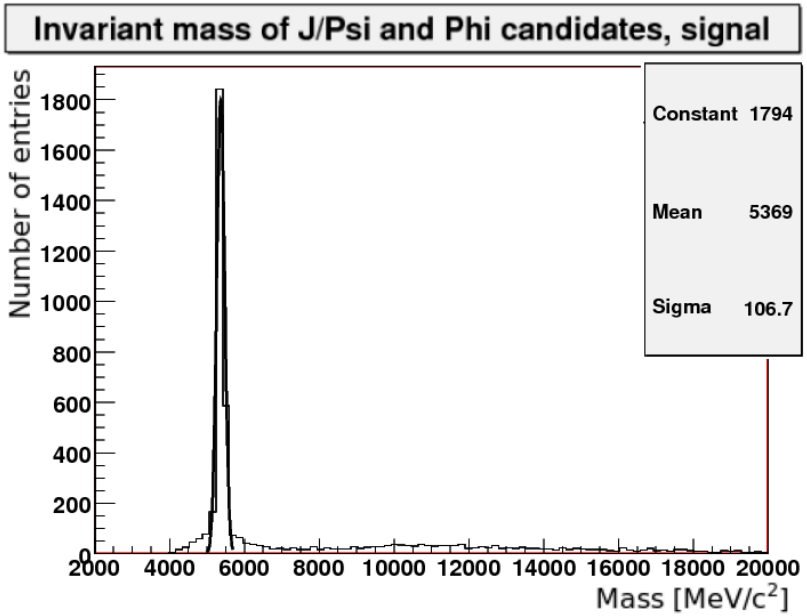

The mean mass and standard deviation from the Gaussian fit are:
$\mu_{B_s} = (5368.7 \pm 2.1)$ MeV , $\sigma_{B_s} = (106.7 \pm 1.5)$ MeV.

Reconstructed B_s Mass from the Signal

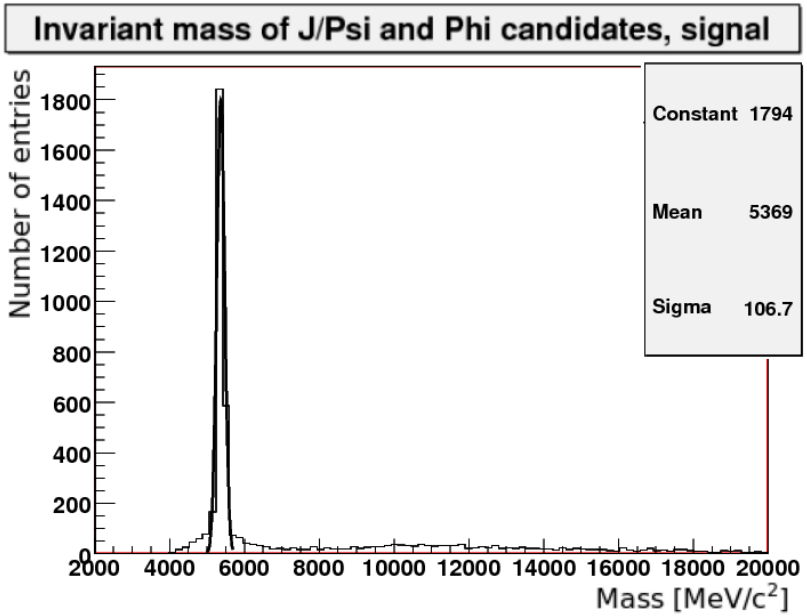

The mean mass and standard deviation from the Gaussian fit are:
$\mu_{B_s} = (5368.7 \pm 2.1)$ MeV , $\sigma_{B_s} = (106.7 \pm 1.5)$ MeV.

This is slightly higher than the PDG value:
$m_{B_s} = (5366.3 \pm 0.6)$ MeV.

Adding Backgrounds

- 2 relevant types of background is added:

Adding Backgrounds

- 2 relevant types of background is added:
  - Generic B background:
    143,750 $bb \rightarrow \mu^+\mu^- X$ or $bb \rightarrow J/\psi(\mu^+\mu^-)X$ events.

Adding Backgrounds

- 2 relevant types of background is added:
  - Generic B background:
    143,750 $bb \rightarrow \mu^+\mu^- X$ or $bb \rightarrow J/\psi(\mu^+\mu^-)X$ events.
  - Direct J/ψ background:
    40,425 $pp \rightarrow J/\psi(\mu^+\mu^-)X$ events.

Adding Backgrounds

- 2 relevant types of background is added:
  - Generic B background:
    143,750 $bb \rightarrow \mu^+\mu^- X$ or $bb \rightarrow J/\psi(\mu^+\mu^-)X$ events.
  - Direct J/ψ background:
    40,425 $pp \rightarrow J/\psi(\mu^+\mu^-)X$ events.
- For the ratio between the signal events and the different background events to mimic that of real data, we introduce a weighting scheme for the background samples:

$$w = a \cdot \frac{\int \text{initial signal histogram}}{\int \text{initial background histogram}}$$

Reconstructed B_s Mass from the Combined Sample

The $\mu^+\mu^- K^+K^-$ invariant mass is reconstructed from the combined signal plus weighted background samples:

Reconstructed B_s Mass from the Combined Sample

The $\mu^+\mu^- K^+K^-$ invariant mass is reconstructed from the combined signal plus weighted background samples:

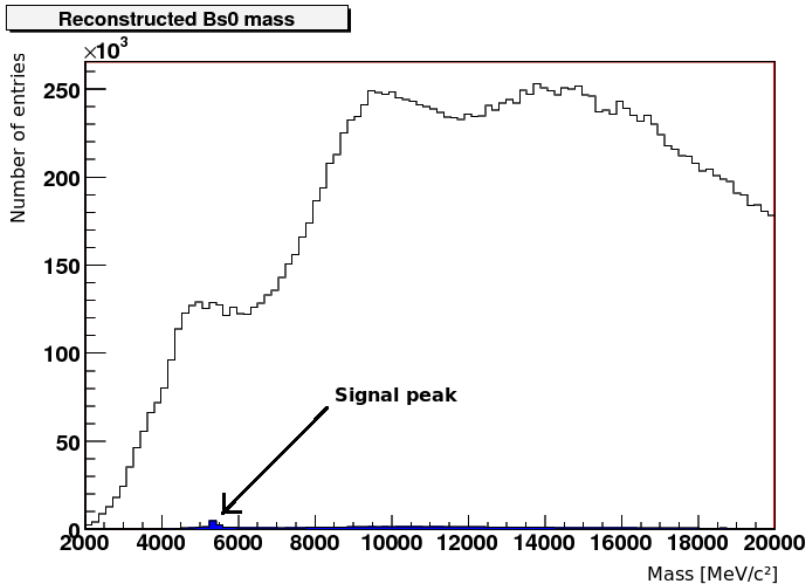

Figure: The reconstructed B_s mass before any selection criteria is imposed

Signal Selection

- Start by introducing some simple selection criteria:

Signal Selection

- Start by introducing some simple selection criteria:

Observable	**Criteria**
Muon transverse momentum	$\geq 4 + 6$ GeV
Fit of muon tracks, χ^2/dof	< 4.0
J/ψ mass	$\mu \pm 3\sigma$ (from fit)
Best pointing angle of B_s	—

Signal Selection

- Start by introducing some simple selection criteria:

Observable	**Criteria**
Muon transverse momentum	$\geq 4 + 6$ GeV
Fit of muon tracks, χ^2/dof	< 4.0
J/ψ mass	$\mu \pm 3\sigma$ (from fit)
Best pointing angle of B_s	—

- In addition, the following variables look promising:
  - Pointing angle

Signal Selection

- Start by introducing some simple selection criteria:

Observable	**Criteria**
Muon transverse momentum	$\geq 4 + 6$ GeV
Fit of muon tracks, χ^2/dof	< 4.0
J/ψ mass	$\mu \pm 3\sigma$ (from fit)
Best pointing angle of B_s	—

- In addition, the following variables look promising:
  - Pointing angle
  - B_s transverse vertex displacement

Signal Selection

- Start by introducing some simple selection criteria:

Observable	**Criteria**
Muon transverse momentum	$\geq 4 + 6$ GeV
Fit of muon tracks, χ^2/dof	< 4.0
J/ψ mass	$\mu \pm 3\sigma$ (from fit)
Best pointing angle of B_s	—

- In addition, the following variables look promising:
  - Pointing angle
  - B_s transverse vertex displacement
  - Kaon transverse momentum.

Signal Selection

- Start by introducing some simple selection criteria:

Observable	**Criteria**
Muon transverse momentum	$\geq 4 + 6$ GeV
Fit of muon tracks, χ^2/dof	< 4.0
J/ψ mass	$\mu \pm 3\sigma$ (from fit)
Best pointing angle of B_s	—

- In addition, the following variables look promising:
  - Pointing angle
  - B_s transverse vertex displacement
  - Kaon transverse momentum.
  - B_s vertex quality

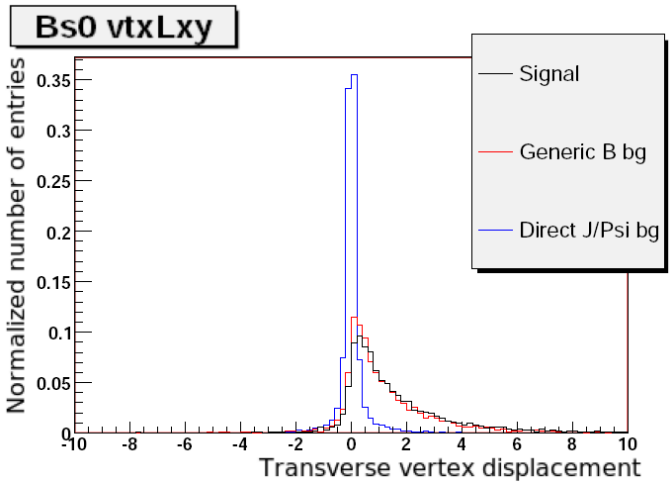
Bs0 vtxLxy
Signal
Generic B bg
Direct J/Psi bg
Normalized number of entries
Transverse vertex displacement

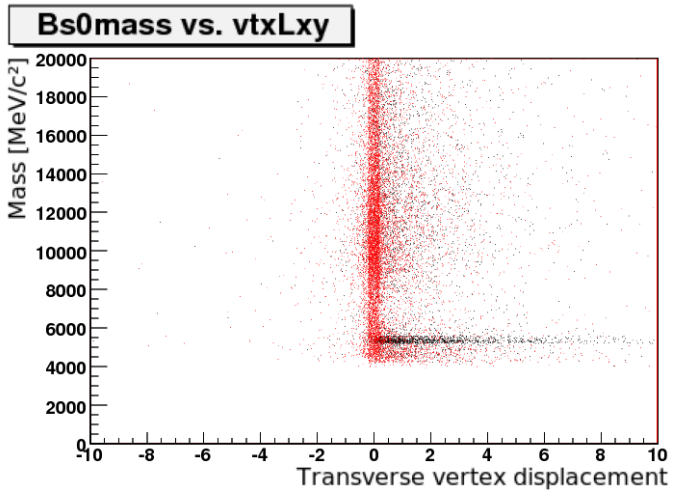
Bs0mass vs. vtxLxy
Mass [MeV/c²]
Transverse vertex displacement

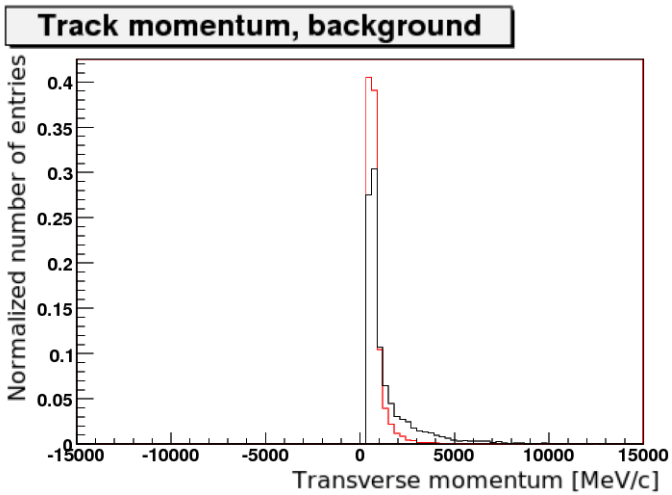
Track momentum, background
Normalized number of entries
Transverse momentum [MeV/c]

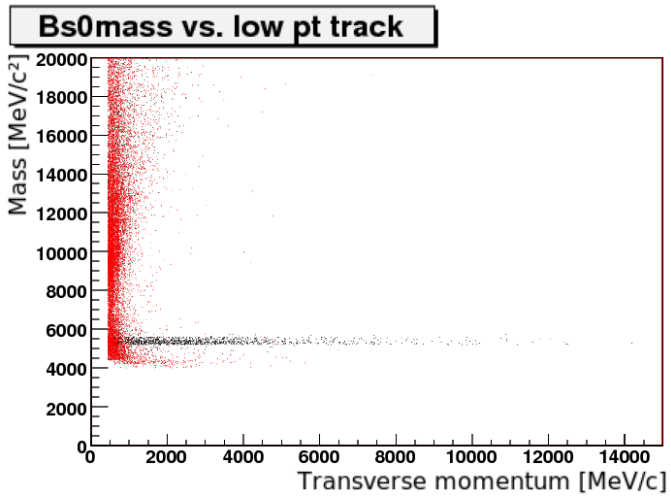
Bs0mass vs. low pt track
Mass [MeV/c²]
Transverse momentum [MeV/c]

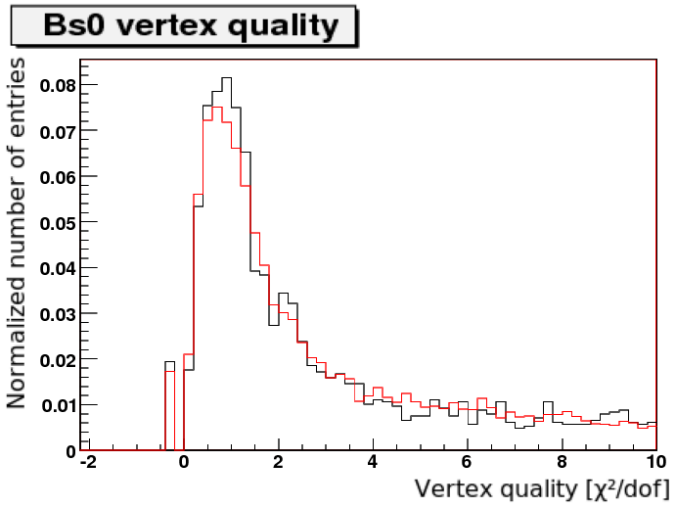
Bs0 vertex quality
Normalized number of entries
Vertex quality [χ²/dof]

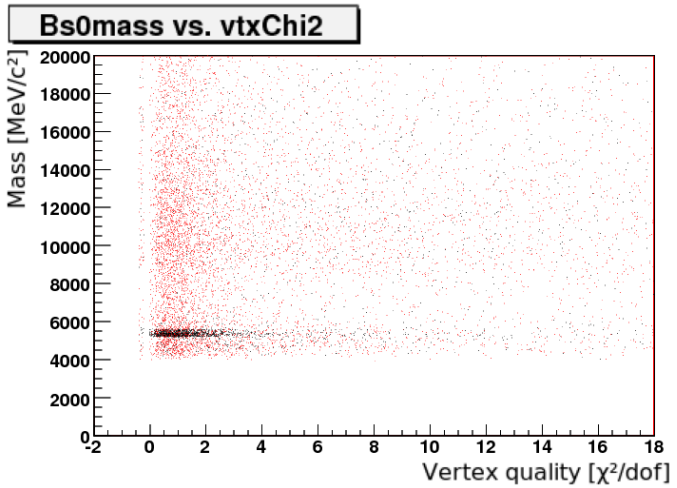
Bs0mass vs. vtxChi2
Mass [MeV/c²]
Vertex quality [χ²/dof]

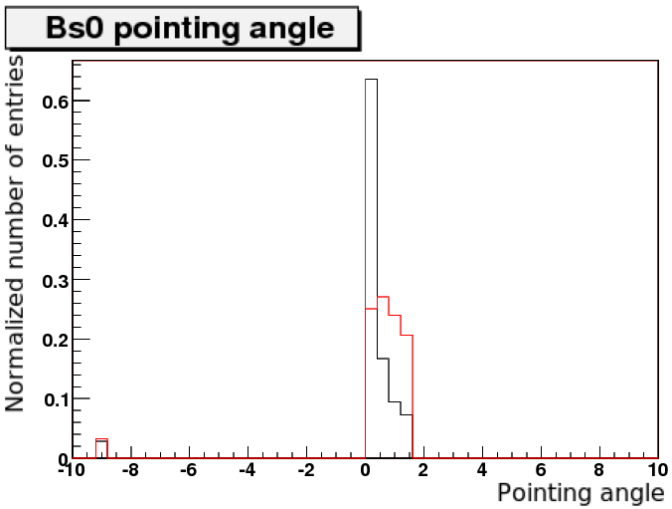
Bs0 pointing angle
Normalized number of entries
Pointing angle

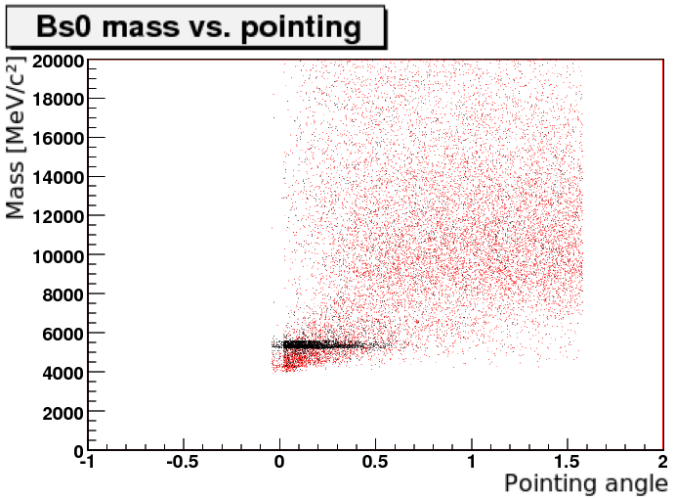
Bs0 mass vs. pointing
Mass [MeV/c²]
Pointing angle

Signal Selection

- To remove as much background as possible while keeping as much of the signal as we can, a parameter known as the sensitivity is introduced:

Signal Selection

- To remove as much background as possible while keeping as much of the signal as we can, a parameter known as the sensitivity is introduced:

$$R = \frac{\#\text{signal events}}{\sqrt{\#\text{signal events} + \#\text{background events}}}$$

Signal Selection

- To remove as much background as possible while keeping as much of the signal as we can, a parameter known as the sensitivity is introduced:

$$R = \frac{\#\text{signal events}}{\sqrt{\#\text{signal events} + \#\text{background events}}}$$

- Only the mass window between 5100 MeV and 5700 MeV is considered.

Signal Selection

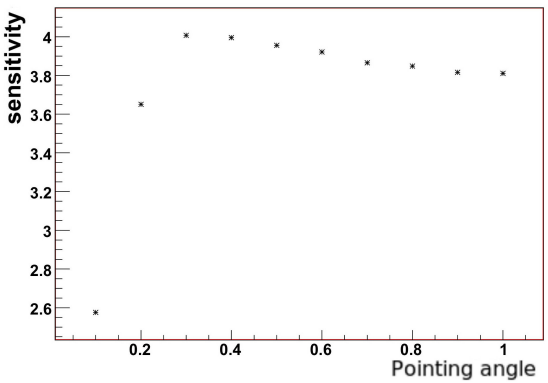

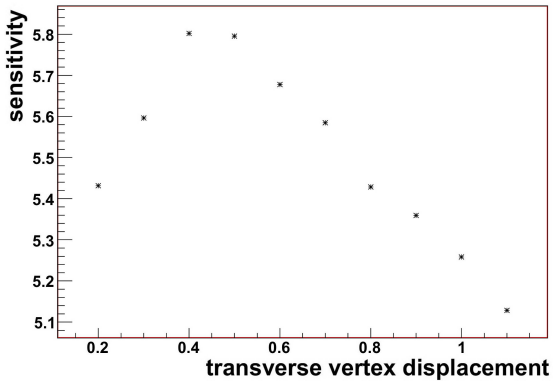

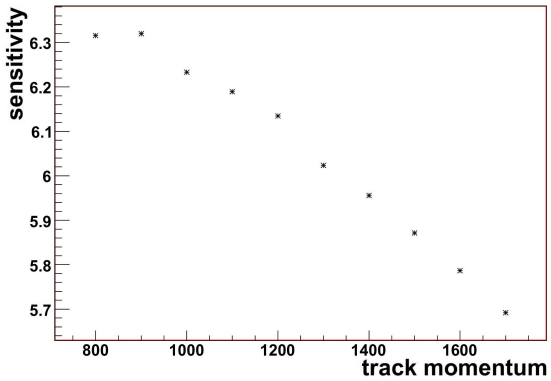

When calculating the sensitivity we have assumed an integrated luminosity of 1 fb^{-1}.

Signal Selection

Based on the sensitivity plots, we employ the following criteria in addition to the ones already mentioned:

Signal Selection

Based on the sensitivity plots, we employ the following criteria in addition to the ones already mentioned:

Observable	**Optimized Criteria**	**Sensitivity**
Pointing angle of B_s	≤ 0.3	4.01
Transverse vertex displacement	≥ 0.4	5.80
Kaon transverse momentum	≥ 0.9 GeV	6.32

Signal Selection

Based on the sensitivity plots, we employ the following criteria in addition to the ones already mentioned:

Observable	**Optimized Criteria**	**Sensitivity**
Pointing angle of B_s	≤ 0.3	4.01
Transverse vertex displacement	≥ 0.4	5.80
Kaon transverse momentum	≥ 0.9 GeV	6.32

The table also lists the sensitivity obtained after each new criteria is introduced.

Reconstructed B_s Mass from the Combined Sample

The reconstructed $\mu^+\mu^- K^+K^-$ invariant mass after optimizing the selection criteria and including an additional cut on the ϕ mass:

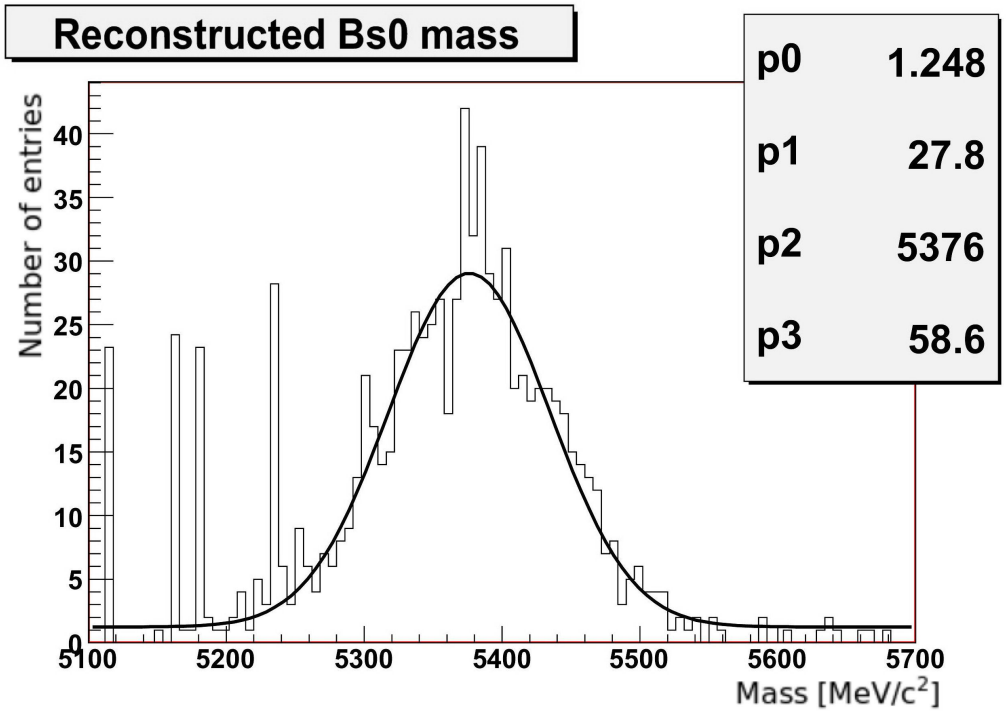

Reconstructed B_s Mass from the Combined Sample

The reconstructed $\mu^+\mu^- K^+K^-$ invariant mass after optimizing the selection criteria and including an additional cut on the ϕ mass:

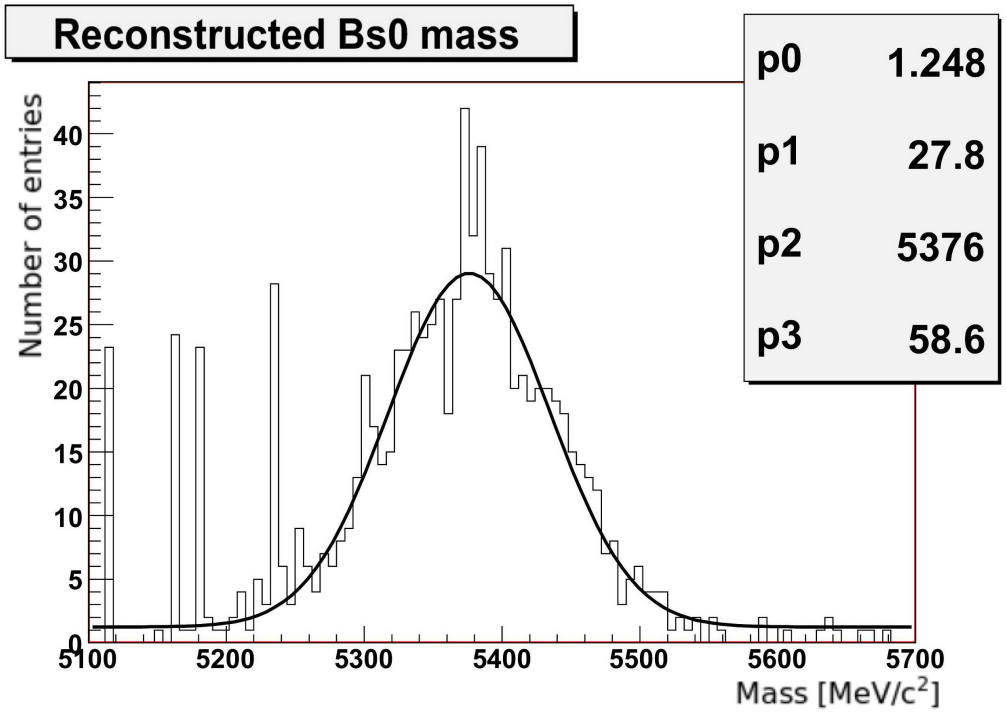

From the fit we obtain the following mean mass and standard deviation: $\mu_{B_s} = (5376.2 \pm 2.6)$ MeV , $\sigma_{B_s} = (58.6 \pm 2.4)$ MeV.

Summary and Conclusions

- We have performed a validation study using simulated $J/\psi \rightarrow \mu^+\mu^-$ events and looked for variations in the invariant mass distribution for various regions of the ATLAS detector.

Summary and Conclusions

- We have performed a validation study using simulated $J/\psi \rightarrow \mu^+\mu^-$ events and looked for variations in the invariant mass distribution for various regions of the ATLAS detector.
- It was shown that the mass increases at larger values of $|\eta|$, while only minor fluctuations were present as a function of $|\phi|$.

Summary and Conclusions

- We have performed a validation study using simulated $J/\psi \to \mu^+\mu^-$ events and looked for variations in the invariant mass distribution for various regions of the ATLAS detector.
- It was shown that the mass increases at larger values of $|\eta|$, while only minor fluctuations were present as a function of $|\phi|$.
- A separate study was performed to reconstruct the B_s mass using $B_s \to J/\psi\phi \to \mu^+\mu^- K^+K^-$ events.

Summary and Conclusions

- We have performed a validation study using simulated $J/\psi \rightarrow \mu^+\mu^-$ events and looked for variations in the invariant mass distribution for various regions of the ATLAS detector.
- It was shown that the mass increases at larger values of $|\eta|$, while only minor fluctuations were present as a function of $|\phi|$.
- A separate study was performed to reconstruct the B_s mass using $B_s \rightarrow J/\psi\phi \rightarrow \mu^+\mu^- K^+K^-$ events.
- 2 separate types of backgrounds were investigated, and it was shown that by applying some simple selection criteria, we could separate these from the signal.

Summary and Conclusions

- We have performed a validation study using simulated $J/\psi \rightarrow \mu^+\mu^-$ events and looked for variations in the invariant mass distribution for various regions of the ATLAS detector.
- It was shown that the mass increases at larger values of $|\eta|$, while only minor fluctuations were present as a function of $|\phi|$.
- A separate study was performed to reconstruct the B_s mass using $B_s \rightarrow J/\psi\phi \rightarrow \mu^+\mu^- K^+K^-$ events.
- 2 separate types of backgrounds were investigated, and it was shown that by applying some simple selection criteria, we could separate these from the signal.
- The obtained mass after an optimized selection was (5376.2 $\pm$ 2.6) MeV with a (58.6 $\pm$ 2.4) MeV standard deviation.

Summary and Conclusions

- We have performed a validation study using simulated $J/\psi \to \mu^+\mu^-$ events and looked for variations in the invariant mass distribution for various regions of the ATLAS detector.
- It was shown that the mass increases at larger values of $|\eta|$, while only minor fluctuations were present as a function of $|\phi|$.
- A separate study was performed to reconstruct the B_s mass using $B_s \to J/\psi\phi \to \mu^+\mu^- K^+K^-$ events.
- 2 separate types of backgrounds were investigated, and it was shown that by applying some simple selection criteria, we could separate these from the signal.
- The obtained mass after an optimized selection was (5376.2 $\pm$ 2.6) MeV with a (58.6 $\pm$ 2.4) MeV standard deviation.
- The expected value of $m_{B_s} = (5366.3 \pm 0.6)$ MeV is lower, but it was explained that this is due to an over-correction in the muon reconstruction algorithms.

Thank you!

Summary

We have successfully separated the signal from the background using the following simple selection criteria:

Observable	**Criteria**
Muon transverse momentum	$\geq 4 + 6$ GeV
Fit of muon tracks, χ^2/dof	< 4.0
J/ψ mass	$\mu \pm 3\sigma$ (from fit)
ϕ mass	$\mu \pm 2\sigma$ (from fit)
Best pointing angle of B_s	—
Pointing angle of B_s	≤ 0.3
Transverse vertex displacement	≥ 0.4
Kaon transverse momentum	≥ 0.9 GeV

Summary

The obtained B_s mass $\mu_{B_s} = (5376.2 \pm 2.6)$ MeV
and standard deviation $\sigma_{B_s} = (58.6 \pm 2.4)$ MeV.
Compared to the expected value, $m_{B_s} = (5366.3 \pm 0.6)$ MeV, the obtained mass is slightly high.
This is due to an over-correction in the muon reconstruction algorithms.

Back-up slides

LHC Injection Chain

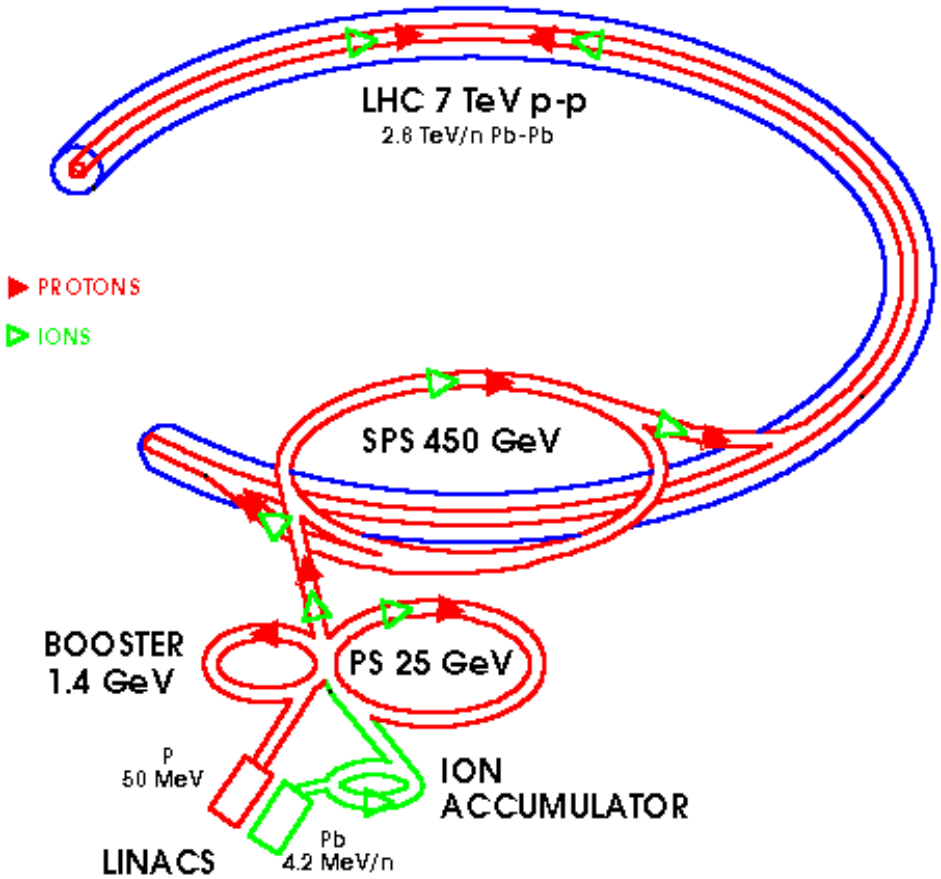

Magnets

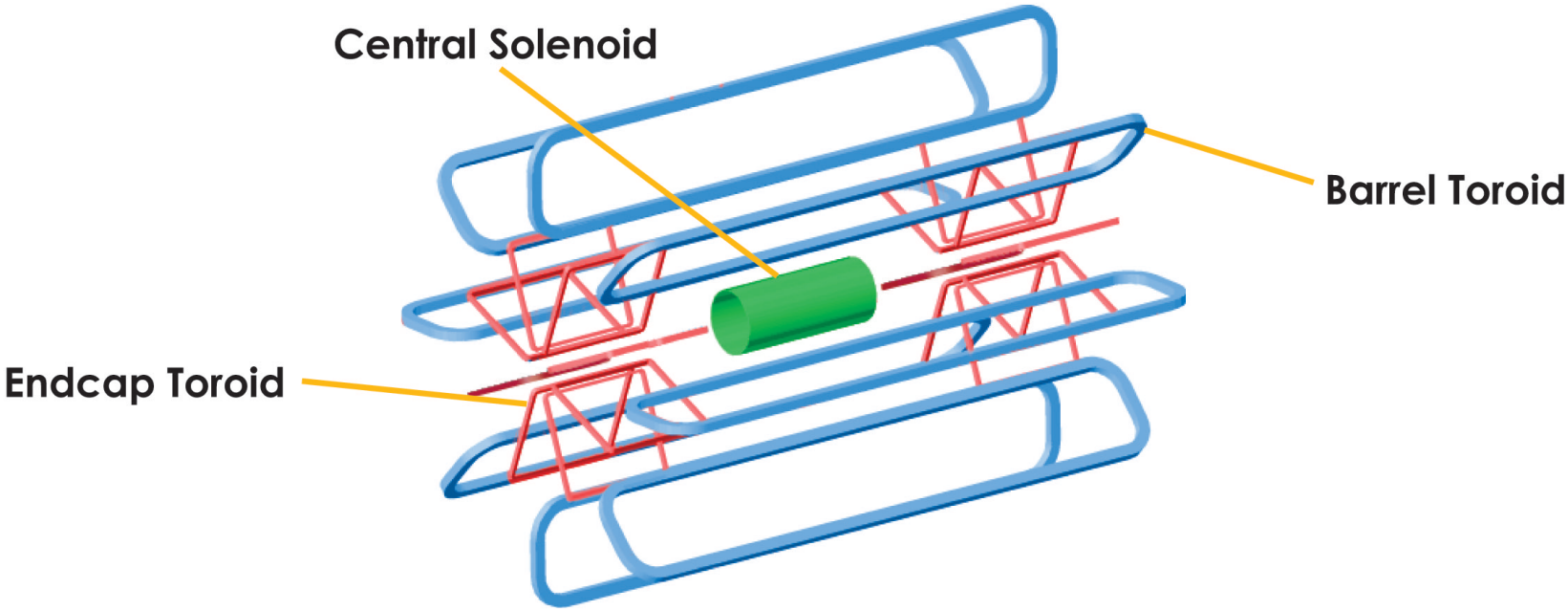

Inner Detector

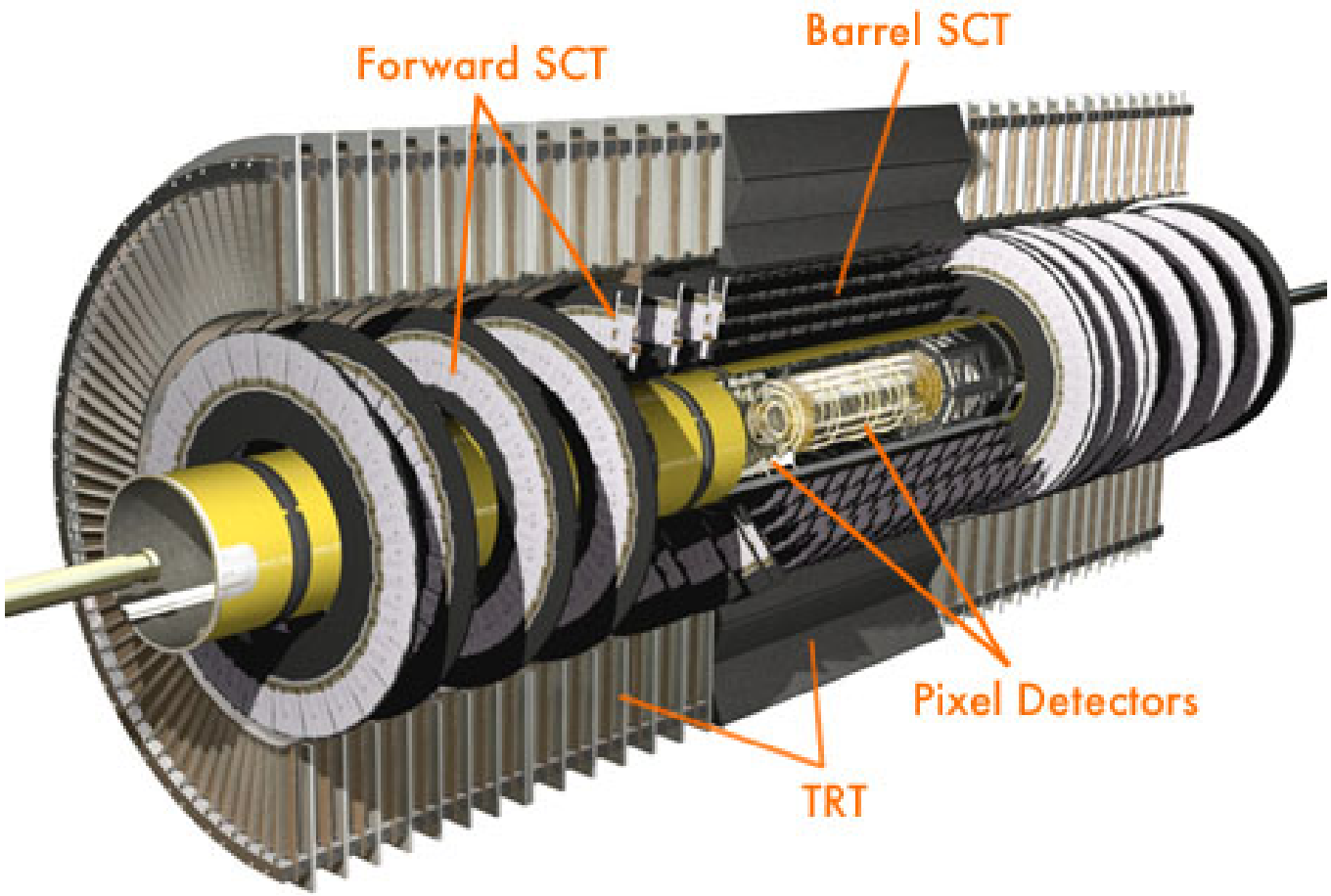

Calorimeters

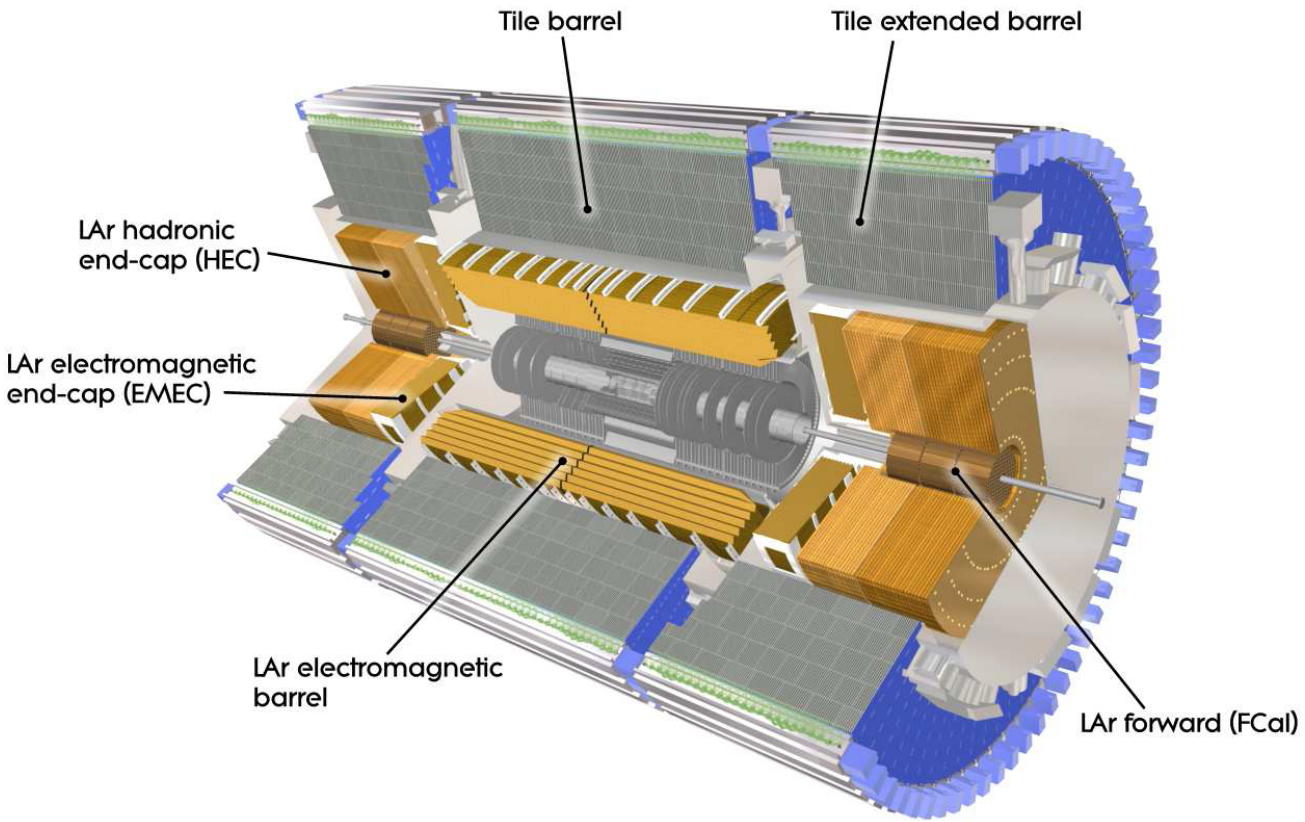

Muon Spectrometers

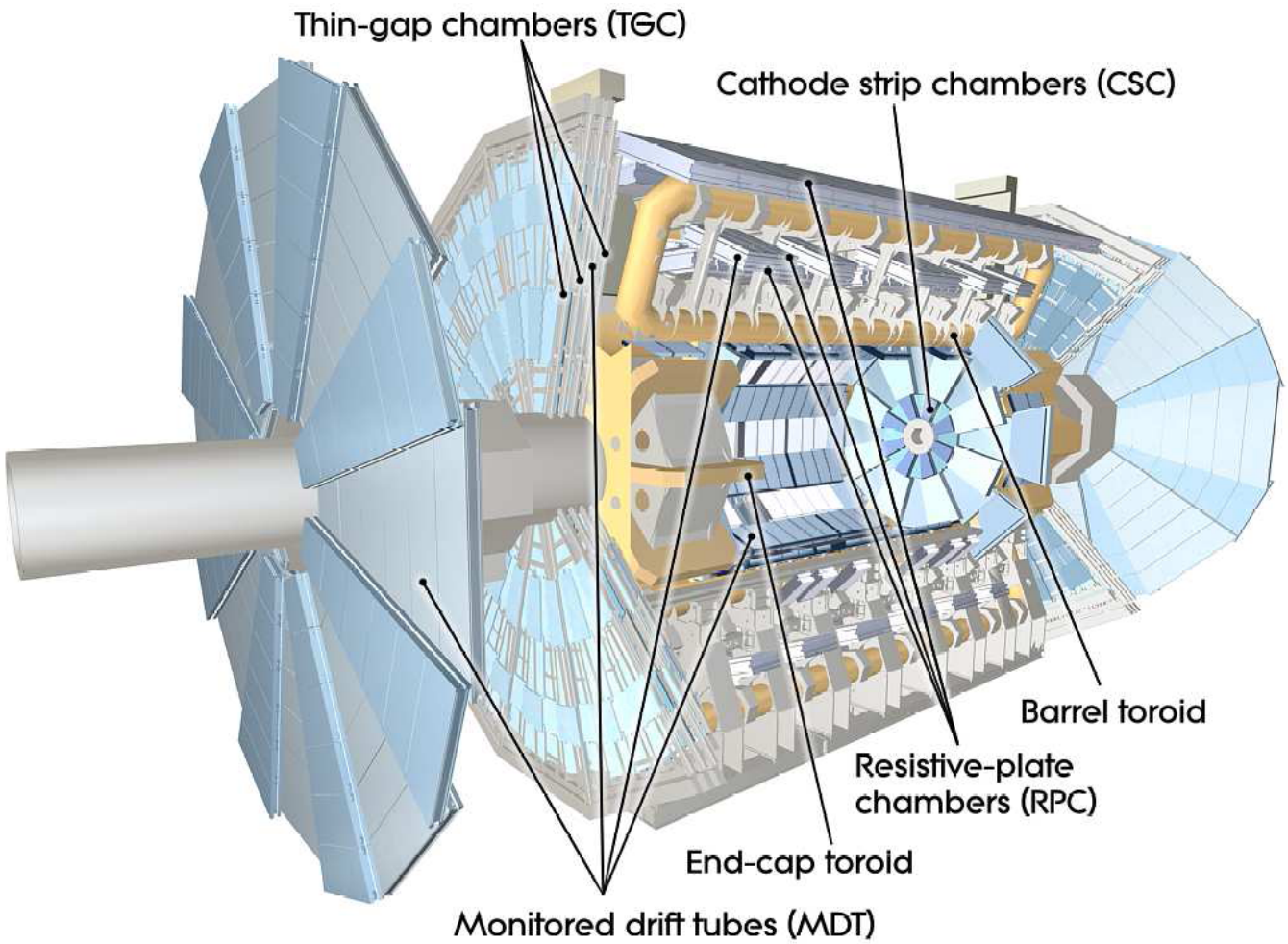

Muon Spectrometers

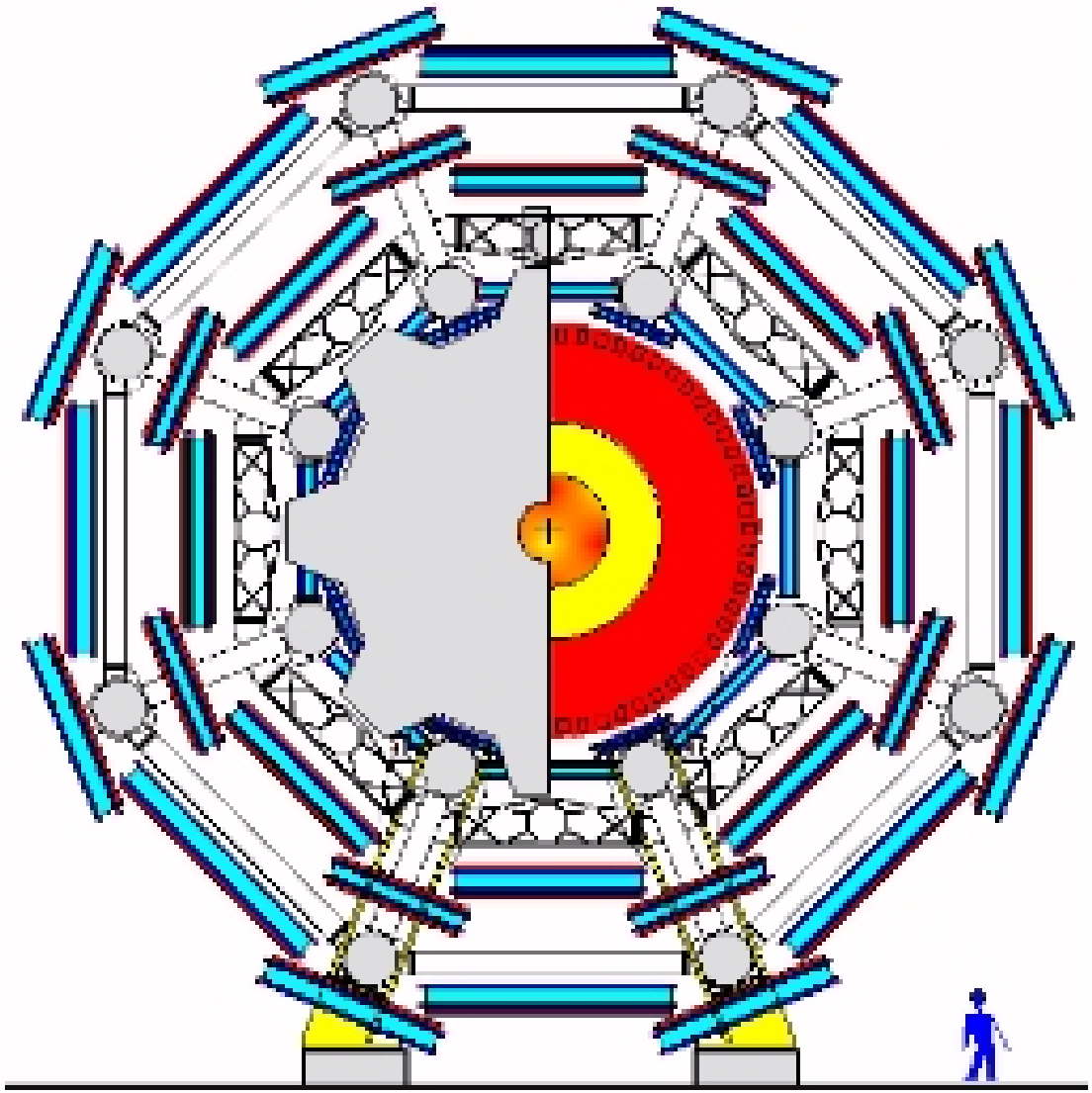

Trigger System

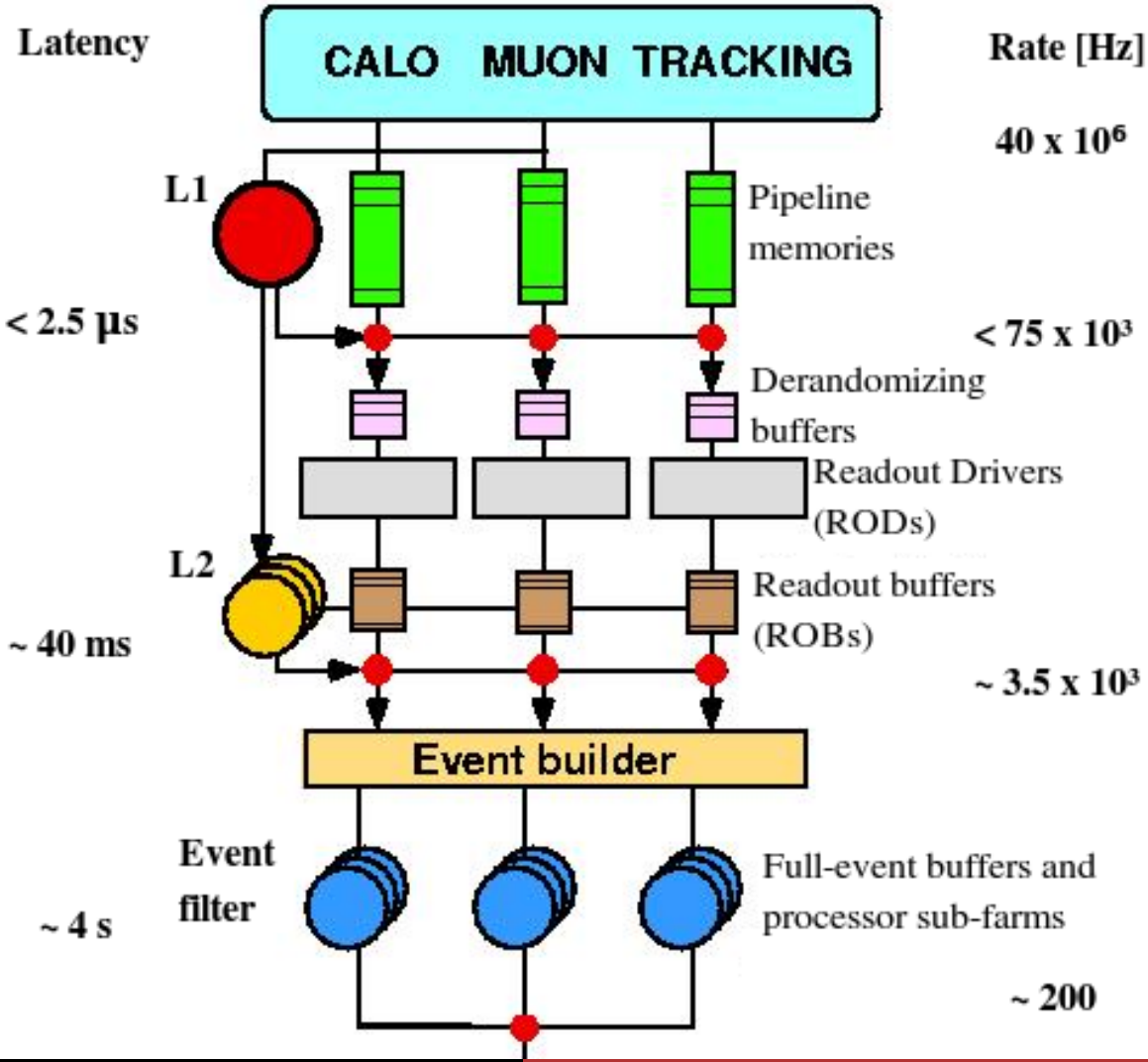

Cosmic Muon Event in SCT/TRT